Quasielastic Neutron-Scattering Study of the Local Dynamics of Poly(ethylene glycol) Dimethyl Ether in Aqueous Solution

Frans R. Trouw,*,† Oleg Borodin,‡ Jeremy C. Cook,§ John R. D. Copley,§ and Grant D. Smith‡

Manuel Lujan Jr. Neutron Scattering Center, Los Alamos National Laboratory, P.O. Box 1663, MS H805, Los Alamos, New Mexico 87545, Department of Materials Science and Engineering and Department of Chemical & Fuels Engineering, 122 S. Central Campus Drive, University of Utah, Salt Lake City, Utah 84112, and NIST Center for Neutron Research, 100 Bureau Drive, Stop 8562, Gaithersburg, Maryland 20899-8562

Received: May 6, 2003; In Final Form: June 26, 2003

Neutron quasielastic scattering experiments were carried out on aqueous solutions of 500 u molecular weight poly(ethylene glycol) dimethyl ether (PEG-DME) in deuterated water. The intermediate scattering functions extracted from the measured neutron scattering can be fitted by a combination of a fast second-order exponential decay ($t < 2$ ps) and a slower first-order exponential decay. The analysis of the momentum transfer (Q) dependence of the decay constant for the slower component shows that it has an approximately constant value at Q's less than 13 nm^{-1} and then increases linearly up to the highest momentum transfer (25 nm^{-1}). Both the slope of the higher-Q linear region and the individual Q-dependent decay constants show a minimum in the PEG-DME weight fraction range of 0.6−0.9. Further analysis of the neutron-scattering data to check the effect of multiple scattering in the sample shows that only the shape of the fast decay ($t < 2$ ps) is affected by this correction. A direct quantitative comparison is made between experiment and molecular dynamics simulations. Fourier transforming the experimental data from the frequency domain into the time domain to yield the intermediate scattering function allows for a quantitative comparison with the equivalent function calculated from the simulations. Furthermore, a Monte Carlo simulation of the experiment based on simulation results is used to account for the effect of multiple scattering quantitatively, which represents a novel approach to dealing with the complications arising from multiple scattering. This correction is significant, resulting in excellent agreement between experiment and the simulations. Both simulation and experiment give rise to a maximum in the relaxation time for PEG-DME proton motion in the PEG-DME weight fraction range of 0.6−0.9. On the basis of the simulations, this maximum arises from competition between the slowing down of the torsional transitions due to hydrogen bonding between the water and the PEG-DME ether oxygens, and the addition of a sufficient quantity of water results in an increasing fraction of large water clusters and more mobile water (i.e., a low-viscosity solvent). The former dominates at low dilution, and the latter dominates at higher dilution, leading to the enhanced backbone motion of the PEG-DME and the observed maximum in the residence time of the PEG-DME protons as a function of composition.

Introduction

Poly(ethylene glycol) (PEG) is an interesting material because the (CH_2CH_2O) monomer is of considerable importance in a large number of applications. For example, polyoxyalkylene copolymers based on a combination such as PEG and poly(propylene glycol) are not only important in industry as surfactants[1] but are also of interest in chemical applications such as the synthesis of mesoporous silicates.[2]

There are a number of publications by other groups that deal with the motion of PEG in aqueous solutions[3−6] as studied by quasielastic neutron scattering. The earlier study[3] looked at two PEG compounds (molecular weights of 400 and 1000 u) using carbon tetrachloride, deuterium oxide, and water as a solvent. The solutions were on the whole quite dilute (up to a polymer weight fraction of 0.4), and the energy resolution of the spectrometer was relatively modest (300−500 μeV). One of the main difficulties encountered in that study was the choice of the model scattering law needed to fit the data, in addition to the uncertainty associated with the translational diffusion constant imposed by the moderate energy resolution and minimum momentum transfer (approximately 10 nm^{-1}). A subsequent high-resolution study[5] (energy resolution of 1 μeV) on a high molecular weight deuterated poly(ethylene oxide) (11 400 u) focused on the mobility of the interfacial water. The other two studies[4,6] were published by the same group. The first paper[4] did not use deuterated polymer or heavy water. The second study[6] focused on a PEG material of comparable molecular weight (600 u) to that in the present work and used both deuterium oxide and water. Polymer weight fractions of 0.35 and 0.7 were used, which are in the range of interest for the present work. However, there is not much discussion of the experimental data with deuterium oxide, and there is limited analysis for the samples with hydrogenous PEG and water. Our previous neutron-scattering publications have looked at the dynamics of water in aqueous poly(ethylene glycol) (PEG-DME) solutions[7] and in aqueous solutions of deuterated 1,2-dimethoxy-

* Corresponding author. E-mail: trouw@lanl.gov.
† Los Alamos National Laboratory.
‡ University of Utah.
§ NIST Center for Neutron Research.

10.1021/jp035234u CCC: $25.00
Published on Web 08/27/2003

ethane,[8,9] which is the smallest molecule that is still representative of PEG. Several other publications[10−13] are concerned with the molecular dynamics simulations of aqueous solutions of PEG-DME.

This paper deals with the motion of relatively short PEG-DME molecules (molecular weight approximately 500 u) in aqueous solution as a function of concentration for comparison with the results of recent molecular dynamics simulations.[10−13] The simulations have provided a number of insights into PEG-DME water mixtures. One of the important aspects of the interactions in these solutions is the competition between water−water and water−ether oxygen hydrogen bonding. From the simulations,[11] this causes clustering of the water up to a water weight fraction of 0.5, at which point the water−ether oxygen hydrogen bonding is saturated. There is also very little bridging water bonding between polymer molecules, but rather this occurs between neighboring and second-nearest-neighbor ether oxygens of the same PEG-DME molecule. Another consequence is that the distribution of PEG-DME conformations varies as a function of weight fraction, which is to be expected in light of the importance of water−ether oxygen hydrogen bonding in conjunction with water clustering at high PEG-DME weight fractions.[10] Furthermore, the relaxation times for C−H reorientation and the rate of decay of the incoherent intermediate scattering function in PEG-DME initially increase as a small amount of water is added[12] and then decrease monotonically as more water is added. The minimum in the short-range proton mobility occurs in the PEG-DME weight fraction (W_p) range between 0.78 and 0.90, which corresponds to a hydration-level range of approximately 3.3−6.5 water molecules per PEG-DME molecule. The water molecules initially cause an increase in the heterogeneity of the conformational transitions, with a maximum that occurs at about the same composition range as the maximum in the C−H orientational and incoherent intermediate scattering function relaxation times. However, this increased heterogeneity accounts only for up to 30% of the decrease in the rate-of-decay incoherent intermediate scattering function. In this paper, we will verify experimentally the minimum in the short-range PEG-DME motions in the range of $0.78 < W_p < 0.90$ as predicted by MD simulations.

Neutron quasielastic scattering from hydrogenous PEG-DME with different amounts of added deuterium oxide provides the means to probe selectively the local motion of the PEG-DME hydrogen atoms. The total neutron-scattering cross section for hydrogen is approximately 16 times greater than that of deuterium, so the PEG-DME hydrogen atoms (aside from very dilute solutions) will dominate the measured scattering. Moreover, it is straightforward to calculate the intermediate scattering function from the simulations for a direct comparison with the experimental results.

Experimental Section

Poly(ethylene glycol) dimethyl ether was used for the neutron-scattering experiments because the methyl group termination avoids any potential proton exchange of hydroxyl groups with deuterium oxide. The polymer that was used was relatively polydisperse ($M_w = 470$, $M_n = 398$) as obtained from Aldrich and was used as received. A molecular weight of 398 corresponds to $CH_3-(O-CH_2-CH_2)_8-OCH_3$, and 484 corresponds to $CH_3-(O-CH_2-CH_2)_{10}-OCH_3$. The isotopic purity of the deuterium oxide was >99% deuterium (Aldrich). Measurements were made on the pure PEG-DME and PEG-DME/D_2O mixtures with PEG-DME weight fractions of 0.89, 0.77, 0.62, 0.48, and 0.17. The temperature of the sample was maintained at 318 K during the experiments.

The neutron quasielastic scattering experiments were carried out on the disk chopper spectrometer (DCS) located at the NIST Center for Neutron Research (http://www.ncnr.nist.gov). This direct geometry chopper spectrometer was operated with an incident neutron wavelength of 0.48 nm, which yielded an energy resolution function that is approximately Gaussian in shape with a full width at half-maximum of 105 μeV. One measurement was made on the pure PEG-DME melt with an incident neutron wavelength of 0.75 nm, which gave an energy resolution of 33 μeV. The reduced count rate at the higher-energy resolution made that option less attractive, and the comparison between the two data sets demonstrated that an energy resolution of 105 μeV is quite adequate for exploring the local dynamics in these PEG-DME solutions.

Annular sample geometry was chosen for this experiment to try to reduce the multiple scattering in a thick sample. An aluminum sample can composed of two concentric cans was used, with an approximate diameter of 1.98 cm and an annular gap of 0.04 cm. The sample can was attached to a helium gas closed-circuit refrigerator equipped with a heater to allow for sample control at 318 K.

The beam height was 10 cm, and the beam was masked down to a width of 1.5 cm to avoid the sides of the annulus, which would have increased the amount of multiple scattering. Even with such a masked annular sample, a 0.04-cm sample thickness implies a transmission of approximately 70% and a significant degree of multiple scattering.

The measured neutron-scattering intensities were corrected in the traditional way by subtracting the scattering from the empty can corrected for the different transmissions of the full and empty cans and for the instrument response by correction with the scattering from a vanadium standard. Twenty groups of detectors were chosen, covering a range of momentum transfer from 2 to 24 nm^{-1}. The three lowest Q values were not used in the further analysis of the data because there was significant extra background scattering at those small angles (lowest Q used was 5.3 nm^{-1}). No attempt was made to fit the data in the form of $S(Q, \omega)$; instead, the results were transformed into the intermediate scattering function (ISF), $I(Q, t)$, using the appropriate Fourier transform as described in a previous publication.[9]

The effect of multiple scattering was explored using the MSCAT code developed by Copley.[14] MSCAT is based on a Monte Carlo simulation of the experiment, with an analytical neutron-scattering law as the main input. The basic geometry of the DCS instrument was used in these simulations in conjunction with the experimental specific setup as described above. The scattering law used as input for MSCAT was derived from the intermediate scattering functions obtained from the molecular dynamics simulations. Because MSCAT requires an analytical form for $S(Q, \omega)$ that is defined over a wide range of Q and ω, the ISFs from the simulation were fitted by a sum of four exponential decays, which yielded a set of parameters that could be satisfactorily interpolated over the momentum- and energy-transfer ranges of interest for MSCAT. The resolution function of the spectrometer was not included in the simulations because it can be corrected for in a straightforward manner (convolution in $S(Q, \omega)$ or a multiplication for $I(Q, t)$). MSCAT was then typically run for 100 000 neutrons with a neutron-weight cutoff of 10^{-4} and 5 scattering angles.

MD Simulation Methodology

MD simulations were performed on a mixture of polydisperse oligomers of PEG-DME with the CH_3-capped oligomers of

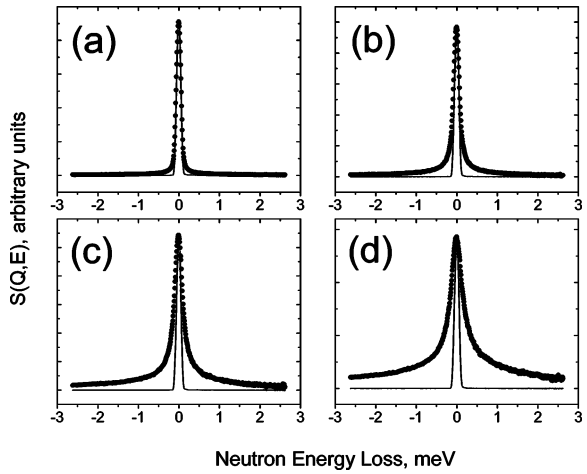

Figure 1. Selection of the corrected neutron-scattering spectra measured for a PEG-DME weight fraction of 0.62 and momentum transfers of (a) 6.38, (b) 12.26, (c) 18.15, and (d) 24.02 nm^{-1}. The narrow peak represents the resolution function of the spectrometer.

ethylene oxide having a structure of $CH_3-(O-CH_2-CH_2)_n-OCH_3$) and water. The PEG-DME molecular weight Schultz−Zimm distribution used in the MD simulations ($M_n = 398$ and $M_w = 475$) is similar to the one for PEG-DME used in the experiments. The total number of ether oxygen atoms in the simulation box was 449. The quantum chemistry-based force fields for PEG[15] and PEG-TIP4P[16] interactions were used in conjunction with a TIP4P water potential.[17]

MD simulations were performed for the following weight fractions (W_p) of PEG-DME: 1.0, 0.89, 0.77, 0.62 and 0.48. The PEG-DME melt and PEG-DME−water $W_p = 0.48$ systems were created in the gas phase. Systems with $W_p = 0.89$, 0.77, 0.62 were derived from the PEG-DME−water system $W_p = 0.48$ by removing water molecules. The box was shrunk in MD simulations using a Brownian dynamics algorithm[18] for 1.5 ns to yield the experimental densities, with subsequent equilibration in an NPT ensemble for 0.5−5 ns using the velocity Verlet algorithm with a 1-fs time step.[19] At each temperature, a 1-ns constant pressure run was carried out to determine the equilibrium density. Subsequent sampling runs in an NVT ensemble were for 10−25 ns. A Nose-Hoover thermostat[20] was used to control the temperature, in combination with a barostat[21] to control the pressure. Bond lengths were constrained using the Shake algorithm.[22] The particle-mesh Ewald (PME) was used to take into account the long-range electrostatic terms.[23] A multiple time step reversible reference system propagator algorithm with three time steps was employed:[21] 0.75 fs for bonding, bending, and torsional motions, a 1.5-fs time step for nonbonded interactions within a 6.5-Å sphere, and a 3.0-fs time step for nonbonded interactions between 6.5 and 10.0 Å and the reciprocal space part of the PME summation.

Results

A representative series of $S(Q, \omega)$ curves collected for $W_p = 0.62$ at 318 K are shown in Figure 1. Also shown is a typical resolution function for the DCS spectrometer as determined by fitting a Gaussian peak shape to the measured vanadium spectra. The extra broadening due to the diffusive motion of the hydrogen atoms of the PEG-DME is self-evident.

No attempt was made to fit the data with a model motion for the PEG-DME protons (e.g., rotational diffusion, jump diffusion, etc.) because it is not clear what the appropriate model might be for such a localized motion in a polymer. From the point of view of the simulations,[12] the intermediate scattering function is best fitted with a stretched exponential decay (the Kohlrausch−Williams−Watts or KWW function that is often invoked for polymers and glasses). There is an approximate form available for the Fourier transform of the KWW decay (i.e., expected form for $S(Q, \omega)$), but such a fit was not attempted.

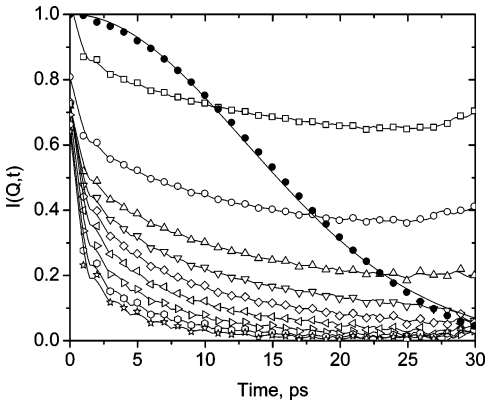

Figure 2. Intermediate scattering functions obtained by an FFT of the neutron-scattering law ($W_p = 0.62$) after correcting for the resolution function of the spectrometer. (Every other point is shown.) The Q values from top to bottom are 5.26, 7.62, 9.94, 12.26, 14.62, 16.99, 19.32, 21.67, and 24.02 nm^{-1}. Also shown is the FFT of the energy resolution function of the DCS spectrometer with an incident neutron wavelength of 0.48 nm (solid points) fitted by a second-order exponential decay (Gaussian).

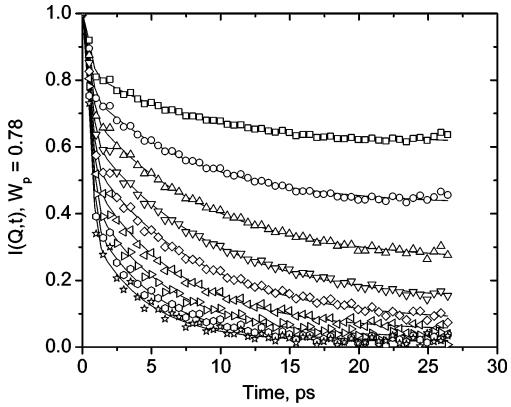

Figure 3. Fits to the intermediate scattering function for $W_p = 0.77$ using a sum of first- and second-order exponential decays plus a constrained background term (same Q values as in Figure 2).

Figure 2 shows the same data for $W_p = 0.62$ after applying the appropriate fast Fourier transform (FFT) and division by the FFT of the equivalent spectrum recorded for the vanadium standard to correct for the energy resolution of the spectrometer (a convolution of the resolution function of the spectrometer in $S(Q, \omega)$ implies a multiplication in $I(Q, t)$). Also shown is the nominally Q-independent energy resolution function in the form of the intermediate scattering function, which demonstrates how the chosen DCS energy resolution of 105 μeV limits the sampling of the single-particle proton density decay to about 30 ps.

An obvious feature of the ISFs is the separation into an early fast decay that is complete within 1−2 ps, followed by a slower decay that extends out to 30 ps and beyond. All of the ISFs can be satisfactorily fitted by the sum of a fast $\exp(-\alpha t^2)$ decay and a slower $\exp(-\beta t)$ decay plus a flat background scaled to force the ISF to unity at $t = 0$. Examples of such a fit to several of the ISFs for $W_p = 0.77$ are shown in Figure 3.

The resulting values for β are plotted as a function of momentum transfer in Figure 4 for the different PEG-DME

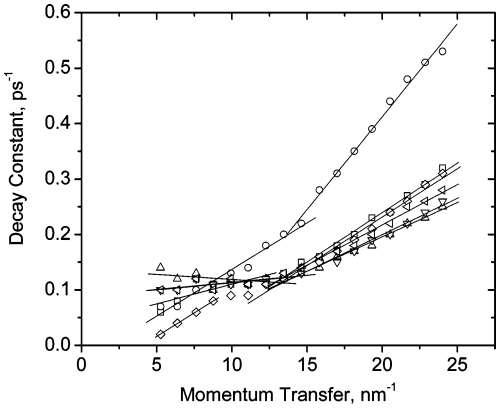

Figure 4. Momentum transfer dependence of the constant β for the slower decay shown in Figure 3. The lines are linear fits to the data, with a break at approximately 13 nm^{-1}.

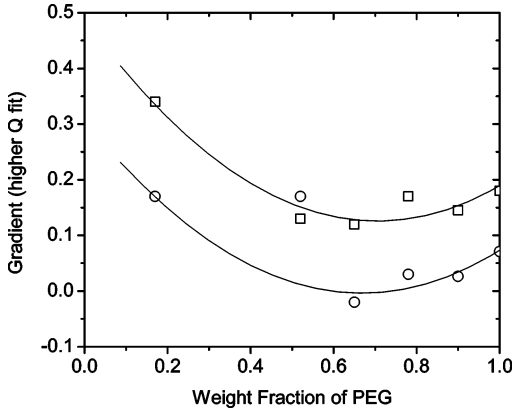

Figure 5. Composition dependence of the higher Q (>13 nm^{-1}, squares) and lower Q (circles) gradients of the lines fitted to the data in Figure 4. The curves are guides for the eye.

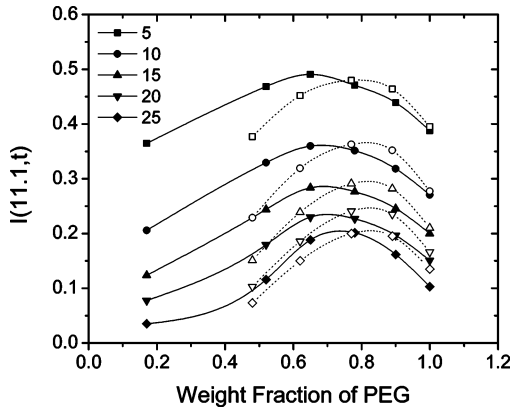

Figure 6. Values of the ISF derived from the DCS experiment at 5, 10, 15, 20, and 25 ps as a function of composition. The equivalent simulation values are shown as open symbols with the dashed line as a guide for the eye.

weight fractions. Decay constant β can be fitted using two straight lines—one from about 5−13 nm^{-1} and the other from 13 to 24 nm^{-1}.

Figure 5 shows how the gradient of the straight line fitted at the higher Q values varies as a function of the weight fraction of PEG-DME.

Figure 6 shows the variation in the value of the ISF at a momentum transfer of 11.1 nm^{-1} as a function of the weight fraction of PEG-DME at 5, 10, 15, 20, and 25 ps. Also shown for comparison is the same variation for the ISFs from the simulation at a momentum transfer of 11.3 nm^{-1}.

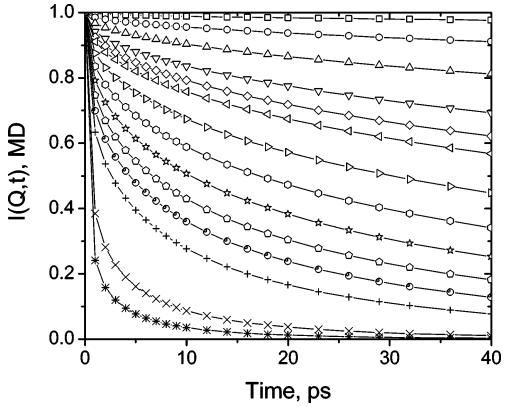

Figure 7. Intermediate scattering functions for a pure PEG-DME melt at 318 K as predicted by simulation.[13] Momentum transfer values from top to bottom are 1, 2, 3, 4, 4.57, 5, 6, 7, 8, 9, 10, 11.39, 17.16, and 21.74 nm^{-1}.

Figure 7 shows the ISFs calculated for $W_p = 1.0$ on the basis of the simulations described in the previous work.[16] Before a comparison can be made between simulation and experiment, it is necessary to quantify the effect of multiple scattering in the neutron experiment. To make as meaningful a comparison as possible, the results of the simulations were used as input for the MSCAT multiple-scattering program. The FFT of the $S(Q, \omega)$ output from MSCAT (i.e., the ISFs) for the case of $W_p = 1.0$ is shown in Figure 8a for five different Q values. There are four data sets shown for each Q value, namely, the original simulation ISF (open circles), the ISF predicted by the MSCAT code based on the interpolation of $S(Q, \omega)$ (dashed line), which should be very similar to the simulation result, the ISF obtained on DCS (filled squares), and the ISF obtained from the total (single plus multiple) scattering (line). Also shown in Figure 8b is the fraction of multiple scattering as a function of neutron energy loss for the detectors at $2\Theta = 90°$ ($Q = 19$ nm^{-1}).

Figure 9 shows the ratio of the ISF obtained from the simulation to the total scattering ISF obtained using MSCAT.

It should be noted that the ISFs obtained from the experimental data have been divided by the vanadium resolution function and then divided by $I(Q, 0)$ for each Q value. In principle, the spectra should be scaled by the integrated vanadium signal in each detector grouping, leaving a Q-dependent intensity variation that results from the Debye−Waller factor. As described in a previous publication,[9] scaling by $I(Q, 0)$ yields a better result than attempting the detailed corrections. The values for $I(Q, 0)$ plotted as a function of momentum transfer are shown in Figure 10, and it can be seen that there is some indication of a broad diffraction peak, particularly for the $W_p = 0.17$ sample. The scaling by $I(Q, 0)$ should be correct in the limit that all of the scattering is incoherent, and the agreement between theory and experiment evident in Figure 8a demonstrates that this is a good approximation. Note that the $I(Q, t)$ values calculated from the simulation are not scaled by a Debye−Waller factor, unlike the experimental data.

Figure 11 shows the comparison between simulation and experiment for polymer weight fractions of 0.89, 0.77, 0.62, and 0.48. As there will have to be a similar correction for multiple scattering, a simpler approach was taken by multiplying the simulation ISF by the factors 0.86, 0.91, 0.95 and 1.26 as determined from Figure 9 at the Q values of 4.6, 9.1, 11.4, and 17.2 nm^{-1} respectively,. The factor for the highest Q of 24.0 nm^{-1} varies rapidly over the time domain up to 30 ps and so no attempt was made to correct for multiple scattering at that Q value.

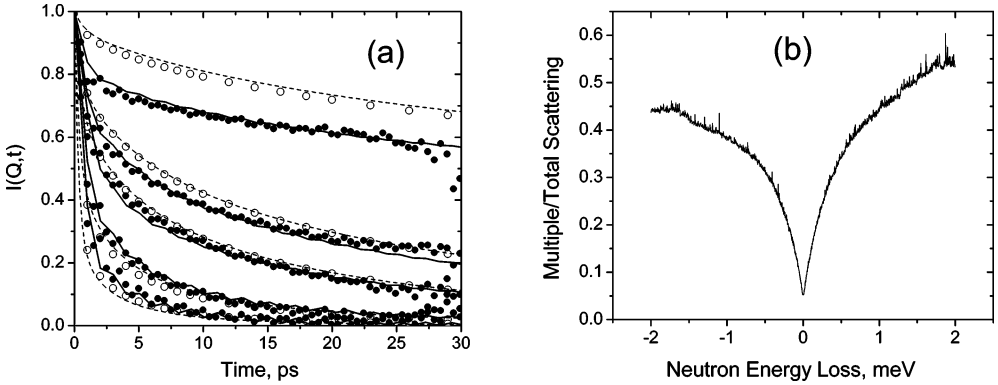

Figure 8. (a) Comparison of the ISF from simulation and experiment. Two curves are shown for each Q value: the original simulation ISF (open circles), the interpolated ideal ISF from MSCAT (dashed line), the ISF including multiple scattering calculated using MSCAT (full line), and the ISF from experiment (filled circles). (b) Ratio of multiple scattering to total scattering as a function of neutron energy loss ($Q = 11$ nm^{-1}).

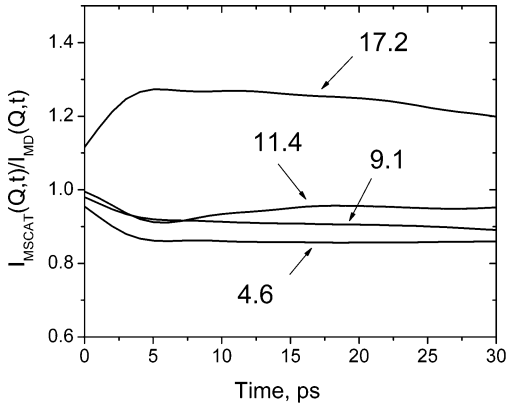

Figure 9. Ratio of the ISF from simulation to the ISF predicted by MSCAT. Q values in nm^{-1} are as indicated.

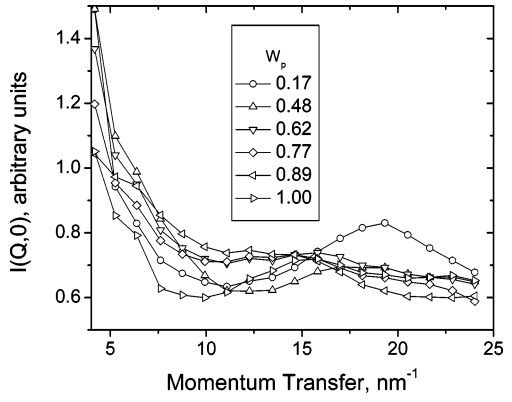

Figure 10. Variation in $I(Q, 0)$ as a function of Q and composition. This is equivalent to the integral over energy of the experimental $S(Q, \omega)$.

Discussion

That two separate time domains are found for all of the ISFs obtained by neutron scattering is not unexpected. A local relaxation of an atom before it encounters the spatial constraints imposed by its neighbors typically takes on the order of a picosecond. This is also the conclusion of previous work on, for instance, polybutadiene and polyisoprene[24] using neutron scattering. Somewhat more surprising is the exponential nature of the second decay, which is frequently found to follow a KWW form (i.e., $\exp[(-t/\tau_{KWW})^{\beta}]$) with a β of typically around 0.2−0.3. Indeed, the ISFs obtained from the simulation of the 12-monomer PEG-DME system[12] could be fitted with the KWW form and $\beta = 0.5-0.6$. That the experimental data does not require a stretched exponential is likely a consequence of the 30-ps limit imposed by the chosen energy resolution of the DCS spectrometer. What this also implies is that attempting to fit the experimental scattering law with the Fourier transform of a stretched exponential would not have been meaningful, being further complicated by the impact of significant multiple scattering.

What is remarkable is the close agreement between simulation and experiment for pure PEG-DME at 318 K as demonstrated in Figure 8. For all of the Q values shown, the agreement is excellent after correcting for multiple-scattering effects. It can also be seen that multiple scattering changes the short-time fast decay of the ISF, particularly at the smaller Q values. These effects are to be expected because multiple scattering will broaden the observed neutron scattering in energy, and the higher scattering angles see more reflected rather than transmitted neutrons. On the basis of this excellent agreement, it can be stated that neutron scattering, for the length and time scales of the experiment, has validated the simulation model.

A conclusion reached in the molecular dynamics simulation paper is that the local motion gives rise to a maximum in the residence time for the C−H orientational autocorrelation function in the range of $W_p = 0.77-0.89$. As can be seen from Figure 5, slow decay constant β for Q's above 13 nm^{-1} has a minimum close to the composition $W_p = 0.77$. Again, this is consistent with the result from the simulations, which is not surprising in light of the excellent absolute agreement between the ISFs from simulation and experiment. This is reinforced by Figure 6, which demonstrates that there is a maximum in the decay of the experimentally derived ISFs for decay times up to 25 ps at a momentum transfer of 11.1 nm^{-1}. A similar maximum is also present for the ISFs obtained from the MD simulations. The two sets are not expected to overlap exactly because the MD results have not been modified to account for multiple scattering.

At this point in the discussion, we have assumed that multiple scattering will not affect the trends found in the analysis. The results for the calculations using MSCAT for the pure PEG-DME as shown in Figure 8 show that the initial decay rate is affected by multiple scattering but that the slower decay rate appears to be essentially unaffected. Figure 9 confirms this, where it can be seen that the ratio is essentially unchanged after about 4 ps, with limiting values in the range of 0.8 to 1.2. The implication of this result is that the decay constants for the slower decay of the ISF will remain unchanged. What is not likely to be correct is the decay constant for the early fast-decay process and the relative intensity scaling between the decay processes.

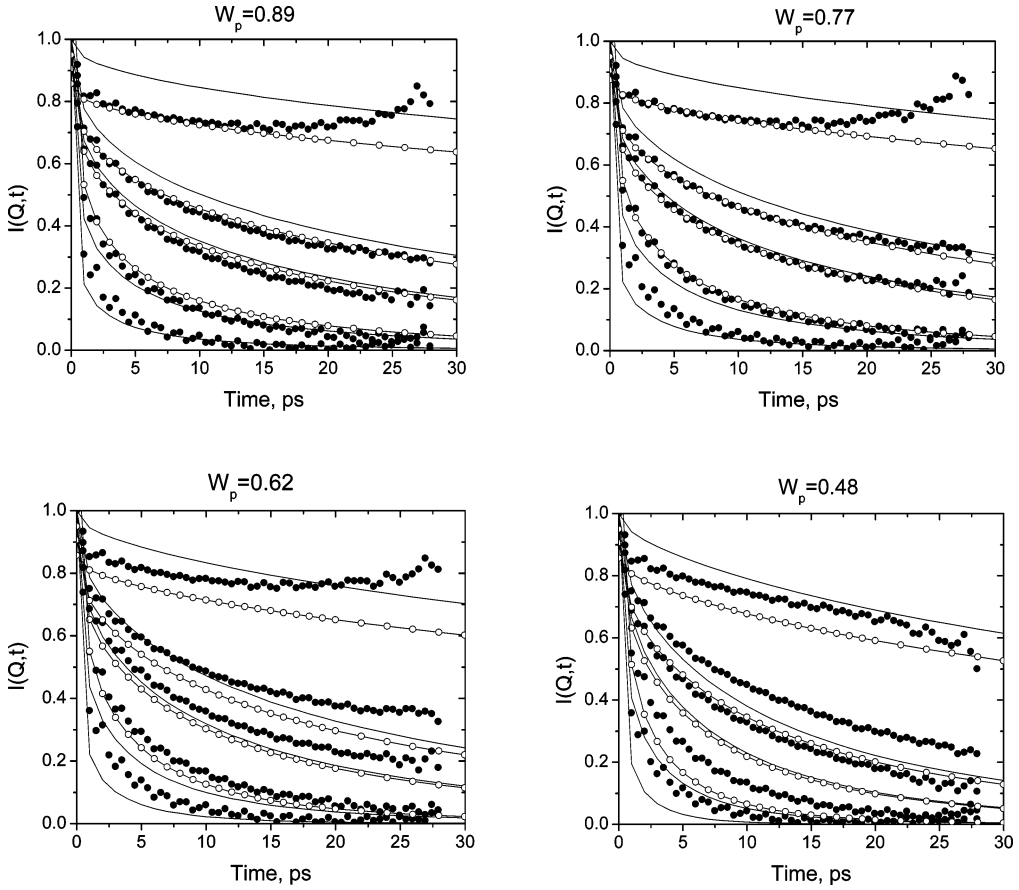

Figure 11. Comparison of ISF from experiment and simulation. The solid line is the simulation ISF, the solid circles are the experimental data, and the line with the open circles is the simulation ISF scaled as described in the text. (Q values in each plot from top to bottom are 4.6, 9.1, 11.4, 17.2, and 24.0 nm^{-1}.)

There is remarkably good agreement with experiment when the simplistic factor correction for multiple scattering is applied to the simulation ISFs at $W_p = 0.89$ and 0.77, indicating that this approximate correction is adequate when only a little deuterium oxide is added. It should be noted that the lowest Q experimental data shown in Figure 11 diverges at longer times, which arises from the slower decay of the ISF at low Q. This means that both the measured ISF and the resolution ISF are small at those times, resulting in a large error and an unphysical upturn in the resolution-corrected ISF. For the weight fractions of 0.62 and 0.48, this simplistic multiple-scattering correction does not improve the agreement between experiment and simulation, and there is some disagreement between simulation and experiment. It can be seen from Figure 11 that the simulation ISF changes more rapidly with the weight fraction of PEG-DME than is the case in the experiment. Some of this disagreement could be a consequence of not correcting for any water scattering at the lower PEG-DME weight fractions, and it is not clear how the results could be corrected for this because the strength and form of the deuterium oxide scattering are not known under these conditions. In other words, subtracting some fraction of the bulk water signal is unlikely to be satisfactory. However, these effects are not sufficient to change the conclusion that there is a maximum in the residence time of the PEG-DME protons as a function of PEG-DME concentration.

Given that the minimum in the decay time of the ISFs at the higher Q's is real, the simulations provide some insight into the reason for this phenomenon. We start by considering the effect of hydrogen bonding on the average time between torsional transitions shown in Figure 12. In agreement with the previous MD simulations of PEG-DME($M_w = 530$)/water,[12] the addition of water forms ether oxygen−water hydrogen bonds, which increases the average time between torsional transitions. This effect is more pronounced for torsions centered on the C−C bond than those for the C−O bond. Because polymer motion in the melt occurs by undergoing torsional transitions, the increased torsional transition time is responsible for slowing down the motion of PEG-DME after the initial addition of water. Further addition of water, however, leads to the formation of large water clusters and ultimately more mobile water, with faster water motion observed with increasing water content as seen in Figure 12 for water rotational reorientation.

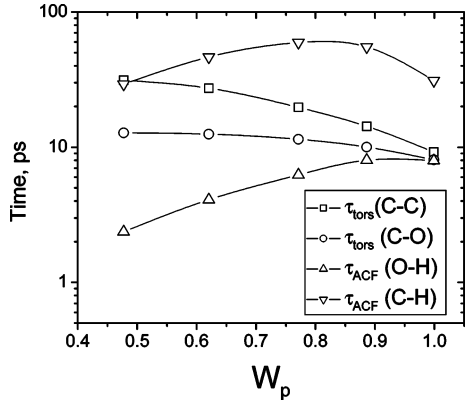

Figure 12. Average time between torsional transitions τ_{tors}, the autocorrelation time for the O−H water bond, and the C−H bond of PEG-DME calculated from the MD simulations as a function of PEG-DME weight fraction.

The water self-diffusion coefficient follows the same trend.[13] An increase in the fraction of highly mobile water increases

the propensity of fragments of PEG-DME and even whole PEG-DME molecules to move in water without undergoing torsional transitions. This mechanism becomes more and more important with increasing PEG-DME dilution and results in faster PEG-DME motions (Figures 5, 6, and 12) at low W_p despite a decreased torsional transition rate of hydrated PEG-DME compared to the one in the melt. It is also interesting that the minimum in PEG-DME dynamics occurs around a concentration corresponding to one water molecule/ether oxygen ($W_p = 0.71$).

Conclusions

The short-range dynamics of aqueous solutions of PEG-DME has been successfully probed using quasielastic neutron scattering. An analysis of the experimental intermediate scattering function for incoherent scattering from the PEG-DME protons shows that there is a fast initial decay that is over in a couple of picoseconds, followed by a slower exponential decay process. This statement is true for all of the different weight fractions of PEG-DME. The slower decay process confirms the prediction from previous molecular dynamics simulations that there is a maximum in the residence time for local proton motion for a composition in the range of $W_p = 0.65-0.9$. This can be understood in terms of two competing mechanism effecting PEG-DME dynamics in water: (a) the formation of ether oxygen−water hydrogen bonds, which slows the torsional transition rate and (b) an increased fraction of quickly diffusing water (solvent), allowing PEG-DME molecules and their segments to diffuse in water without undergoing torsional transitions.

Detailed modeling of the experiment using Monte Carlo techniques to account for the multiple scattering of neutrons in the sample demonstrated that this experimental complication causes a rapid, short time decay of the ISF but that the longer time decay is unaffected. Direct comparisons of the ISFs from simulation and experiment after accounting for multiple scattering show excellent agreement, validating the simulation model on the time and length scales of the experiment.

Acknowledgment. Los Alamos National Laboratory, an affirmative action/equal opportunity employer, is operated by the University of California for the U. S. Department of Energy under contract W-7405-ENG-36. G.D.S. is indebted to the National Science Foundation—Division of Materials Research for support provided through NSF award DMR 0076306. This material is based upon activities supported by the National Science Foundation under agreement DMR-0086210. Any opinions, findings, and conclusions or recommendations expressed are those of the authors and do not necessarily reflect the views of the National Science Foundation. Identification of a commercial product does not imply recommendation or endorsement by the National Institute of Standards and Technology nor does it imply that the product is necessarily the best for the stated purpose.

References and Notes

(1) *Nonionic Surfactants: Polyoxyalkylene Block Copolymers*; Nace, V. M., Ed.; Surfactant Science Series; Marcel Dekker: New York, 1996; Vol. 60.

(2) Zhao, D.; Huo, Q.; Feng, J.; Chmelka, B. F.; Stucky, G. D. *J. Am. Chem. Soc.* **1998**, *120*, 6024.

(3) Dahlborg, U.; Dimic, V.; Cvikl, B. *Phys. Scr.* **1988**, *37*, 93.

(4) Crupi, V.; Jannelli, M. P.; Magazù, S.; Maisano, G.; Majolino, D.; Migliardo, P.; Vasi, C. *Il Nuovo Cimento* **1994**, *16*, 809.

(5) Barnes, A. C.; Bieze, T. W. N.; Enderby, J. E.; Leyte, J. C. *J. Phys. Chem.* **1994**, *98*, 11527.

(6) Crupi, V.; Magazù, S.; Majolino, D.; Migliardo, P.; Wanderlingh, U.; Kagunya, W. W. *Physica B* **1998**, *241−243*, 979.

(7) Borodin, O.; Trouw, F., Bedrov, D.; Smith, G. D. *J. Phys. Chem B* **2002**, *106*, 5184.

(8) Bedrov, D.; Borodin, O.; Smith, G. D.; Trouw, F.; Mayne, C. *J. Phys. Chem. B* **2000**, *104*, 5151.

(9) Trouw, F.; Bedrov, D.; Borodin, O.; Smith, G. D. *Chem. Phys.* **2000**, *261*, 137.

(10) Smith, G. D.; Bedrov, D.; Borodin, O. *J. Am. Chem. Soc.* **2000**, *122*, 9548.

(11) Smith, G. D.; Bedrov, D.; Borodin, O. *Phys. Rev. Lett.* **2000**, *85*, 5583.

(12) Borodin, O.; Bedrov, D.; Smith, G. D. *Macromolecules* **2001**, *34*, 5687.

(13) Borodin, O.; Bedrov, D.; Smith, G. D. *J. Phys. Chem. B* **2002**, *106*, 5194.

(14) Copley, J. R. D. *Comput. Phys. Commun.* **1974**, *7*, 289. Copley, J. R. D. *Comput. Phys. Commun.* **1975**, *9*, 95. Copley, J. R. D.; Verkerk, P.; van Well, A. A.; Fredrikze, H. *Comput. Phys. Commun.* **1986**, *40*, 337.

(15) Borodin, O.; Smith, G. D. *J. Phys. Chem. B* **2003**, *107*, 6801−6812 and Borodin, O.; Douglas, R.; Smith, G. D.; Trouw, F.; Petrucci, S. *J. Phys. Chem. B* **2003**, *107*, 6813−6823.

(16) Smith, G. D.; Borodin, O.; Bedrov, D. *J. Comput. Chem*. **2002**, *23*, 1480−1488.

(17) Jorgensen, W. L.; Chandrasekhar, J.; Madura, J. D.; Impey, R. W.; Klein, M. *J. Chem. Phys.* **1983**, *79*, 926.

(18) Smith, G. D.; Jaffe, R. J.; Yoon, D. Y. *Macromolecules* **1993**, *26*, 298.

(19) Allen, M. P.; Tildesley, D. J. *Computer Simulation of Liquids*; Oxford University Press: New York, 1987.

(20) Nose, S. In *Computer Simulation in Materials Science: Interatomic Potentials, Simulation Techniques, and Applications*; Meyer, N., Pontikis, V., Eds.; Kluwer Academic Publishers: Dordrecht, The Netherlands, 1991; p 21.

(21) Martyna, G. J.; Tuckerman, M.; Tobias, D. J.; Klein, M. L. *Mol. Phys.* **1996**, *87*, 1117.

(22) Ryckaert, J. P.; Ciccotti, G.; Berendsen, H. J. C. *J. Comput. Phys.* **1977**, *23*, 327.

(23) Deserno, M.; Holm, C. *J. Chem. Phys.* **1998**, *109*, 7678.

(24) Zorn, R.; Arbe, A.; Colmenero, J.; Frick, B.; Richter, D.; Buchenau, U. *Phys. Rev. E* **1995**, *52*, 781.